Structure and magnetic properties of $Ln_{0.75}Sr_{0.25}Mn_{0.90}Fe_{0.10}O_3$ (Ln = Nd^{+3}, Sm^{+3},Gd^{+3}, Er^{+3}) perovskite manganite prepared by high energy ball milling

A.G. Mostafa, M.Y. Hassaan and M. A. Motawea*

Mössbauer Laboratory, Physics Department, Faculty of Science, Al-Azhar University, Nasr City 11884, Cairo, Egypt
*abdo_metawea@yahoo.com

Abstract: The following perovskites $Ln_{0.75}Sr_{0.25}Mn_{0.90}Fe_{0.10}O_3$ (Ln = Nd^{+3}, Sm^{+3}, Gd^{+3}, Er^{+3}) have been prepared by by high energy ball milling method. X-ray diffraction (XRD) analyses showed the presence of the single crystalline perovskite phase, orthorhombic system with (Pbnm) space group. The crystallite size and the lattice parameters decrease gradually with substitution Nd^{+3} by Sm^{+3}, Gd^{+3}, or Er^{+3}. Specific surface area increase and Scanning Electron Microscopy, can be see that the particle morphology decrease with substitution Nd^{+3} by Sm^{+3}, Gd^{+3}, or Er^{+3} of $Ln_{0.75}$ $Sr_{0.25}$ $Mn_{0.90}$ $Fe_{0.10}O_3$ (Ln = Nd^{+3}, Sm^{+3}, Gd^{+3}, Er^{+3}). The magnetic measurements showed that soft ferromagnetic materials.

[Mostafa AG., Hassaan MY, Motawea M A. **Structure and magnetic properties of $Ln_{0.75}Sr_{0.25}Mn_{0.90}Fe_{0.10}O_3$ (Ln = Nd^{+3}, Sm^{+3},Gd^{+3}, Er^{+3}) perovskite manganite prepared by high energy ball milling.** *Researcher* 2013;5(3):46-51]. (ISSN: 1553-9865). http://www.sciencepub.net/researcher. 7

Key words: ball milling, perovskites, magnetic properties

1. Introduction

Mixed-valence perovskite manganites with the general formula $R^{3+}_{1-x}A^{2+}_{x}$ $Mn^{3+}_{1-x}Mn^{4+}_{x}$ O^{2-}_{3} where R denotes a rare earth element, and A is an alkali-earth element, have been the subject of intense research interest for several decades, owing to the variety of their unique properties, such as colossal magneto-resistance, ferromagnetic transition accompanied by an insulator–metal transition, giant thermal expansion, charge ordering structures, field-induced structural changes, and pronounced catalytic activity [1–3]. These properties present a vast potential for a wide range of applications: as, materials for magnetic recording heads and sensors, permanent magnets, Ferro fluids, pigments, working substances in magnetic refrigerators and catalysts [3]. In the range of x=0.2–0.4, the ground state of the compound is ferromagnetic, and the paramagnetic–ferromagnetic (PM–FM) transition is accompanied by a sharp drop in receptivity [4, 5].

For x > 0.3, charge order is observed, and competes with the FM state leading to a more complex electronic behavior [6]. The mechano-chemical process appears like an effective, economical and versatile way to produce fine particles. This process is based on chemical reactions mechanically activated by high-energy ball milling [7, 8]. It has been successfully applied to obtain different oxides [9,10]. Recently, the effectiveness of high energy ball milling technique to promote mechano-synthesis (mechanical synthesis method) of fine structured maganite by mechanical activation of chlorides and oxides' compounds to synthesized $Ln_{0.75}$ $Sr_{0.25}$ $Mn_{0.90}$ $Fe_{0.10}O_3$ (Ln = Nd^{+3}, Sm^{+3},Gd^{+3}, Er^{+3}) has been demonstrated [11]. In the present paper, were port the synthesis, structure, nanostructure, and magnetic properties of $Ln_{0.75}Sr_{0.25}Mn_{0.90}Fe_{0.10}O_3$ (Ln = Nd^{+3}, Sm^{+3},Gd^{+3}, Er^{+3}) sample fabricated by ball milling method.

2. Materials and Methods

Ln_2O_3 (Ln = Nd^{+3}, Sm^{+3}, Gd^{+3}, Er^{+3}), $SrCO_3$, MnO_2 and Fe_2O_3 powders were used as raw materials. Ln_2O_3 and $SrCO_3$ were fired at 1173 and 673 K for 6 and 4 h, respectively, to eliminate moisture and CO_2. Ethanol was added into the agate vials as a milling medium with the powder. The mass ratio of balls and raw materials was 10:1. A high-energy ball mill (500 rpm) was used to mill raw materials under air condition for 15 hours. The mixture was dried in air at 100 ^oC to remove the ethanol. In order to prevent from the excessive overheating of the pot, the mixtures were milled for 90 min then interrupted a break of 5 min. Crystal structure of milled samples was determined by the X-ray diffraction with Cu Kά radiation at room temperature. Their morphology was observed with a SEM. Surface areas of the samples were determined through nitrogen gas adsorption at liquid nitrogen temperature were out gassed at 350 ^oC for 0.5 h before each analysis. The magnetic properties of the prepared samples were measured using vibrating sample magnetometer (VSM) at RT where the magnetic field was equal (20 kOe).

3. Results and Discussion

3.1. X-ray diffraction patterns

X-ray diffraction patterns of the $Ln_{0.75}$ $Sr_{0.25}$ $Mn_{0.90}$ $Fe_{0.10}O_3$ (Ln = Nd^{+3}, Sm^{+3}, Gd^{+3} or Er^{+3}) samples are shown in Fig. (1). All the samples are single phase perovskite without any detectable impurity phases. The XRD patterns are indexed on the basis of the

orthorhombic perovskite (Pb nm). The degree of orthorhombicity (a /b ratio) increases from Nd to Er show in Fig. (5) [12]. The lattice parameters, lattice volume and tolerance factor t for all the $Ln_{0.75}$ $Sr_{0.25}$ $Mn_{0.90}$ $Fe_{0.10}O_3$ samples are summarized in Table (1). The lattice parameter and tolerance factor (t) decreases show Figs. (2, 3) and Mn-O-Mn bond angle decrease and the Mn-O bond lengths increases from Ln = Nd^{+3} to Er^{+3} due to a decrease in the ionic radius of the Ln^{3+} ion which makes the perovskite structure more orthorhombic [12]. This can be due to the decrease of the average ionic radius <rA> where the octahedral tilt and rotate to reduce the excess space around the A site [13].

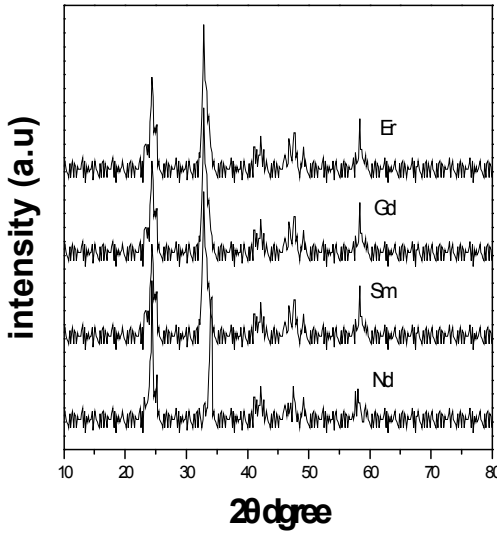

Figure (1). X-ray diffraction patterns of raw materials milled for $Ln_{0.75}Sr_{0.25}Mn_{0.90}Fe_{0.10}O_3$ where Ln is (Nd^{+3}, Sm^{+3}, Gd^{+3} or Er^{+3}).

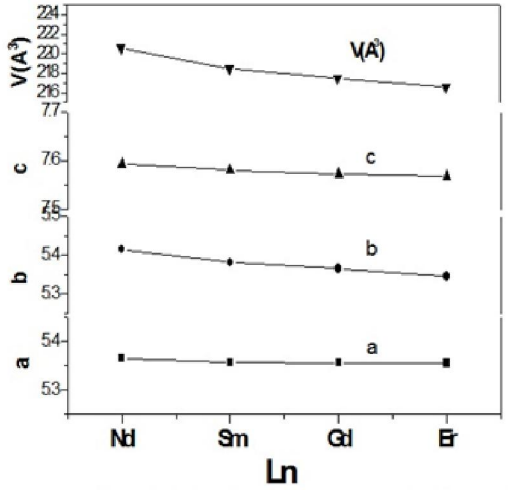

Figure (2) Lattice parameters a, b and c and unit-cell volume for $Ln_{0.75}Sr_{0.25}Mn_{0.90}Fe_{0.10}O_3$ where Ln is (Nd, Sm, Gd or Er).

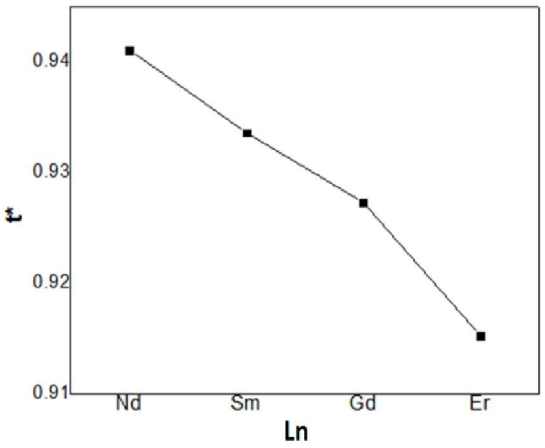

Figure (3). The tolerance factor, t^*, for $Ln_{0.75}$ $Sr_{0.25}$ $Mn_{0.90}$ $Fe_{0.10}O_3$ samples where Ln is (Nd^{+3}, Sm^{+3}, Gd^{+3} or Er^{+3}).

From the Fig. (4) the particle size decrease with the replacement of Nd^{3+} ions by smaller Sm^{3+} ,Gd^{3+} and Er^{+3} ions respectively because of the broken of Mn-O-Mn bonds at the surface of the smaller particles.

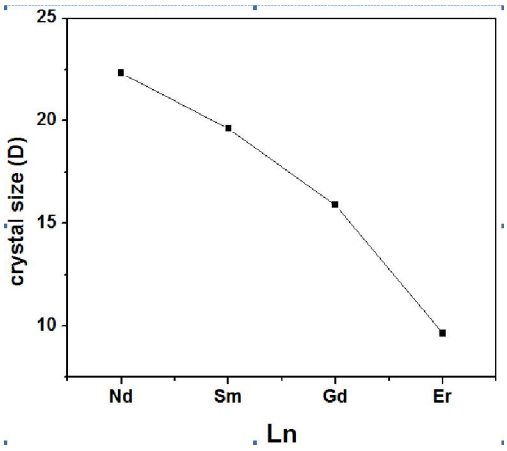

Figure (4). Particle size for $Ln_{0.75}$ $Sr_{0.25}$ $Mn_{0.90}$ $Fe_{0.10}O_3$ samples where Ln is (Nd^{+3}, Sm^{+3}, Gd^{+3} or Er^{+3}).

3.2. Scanning electron microscope (SEM)

SEM micrographs of powder samples for $Ln_{0.75}$ $Sr_{0.25}$ $Mn_{0.90}$ $Fe_{0.10}$ O_3 samples where Ln is (Nd^{+3}, Sm^{+3}, Gd^{+3} or Er^{+3}) are shown in Fig. (6). From this Figure obtained of typical morphology of the $Ln_{0.75}Sr_{0.25}Mn_{0.90}Fe_{0.10}O_3$ samples where Ln is (Nd^{+3}, Sm^{+3}, Gd^{+3} or Er^{+3}) powders, consisting of fine and homogeneous particles. In this Figure with decreasing of the ionic reduce from Nd to Er the grain size decreases. Photos clearly that the particles exist as aggregates of fine grains.

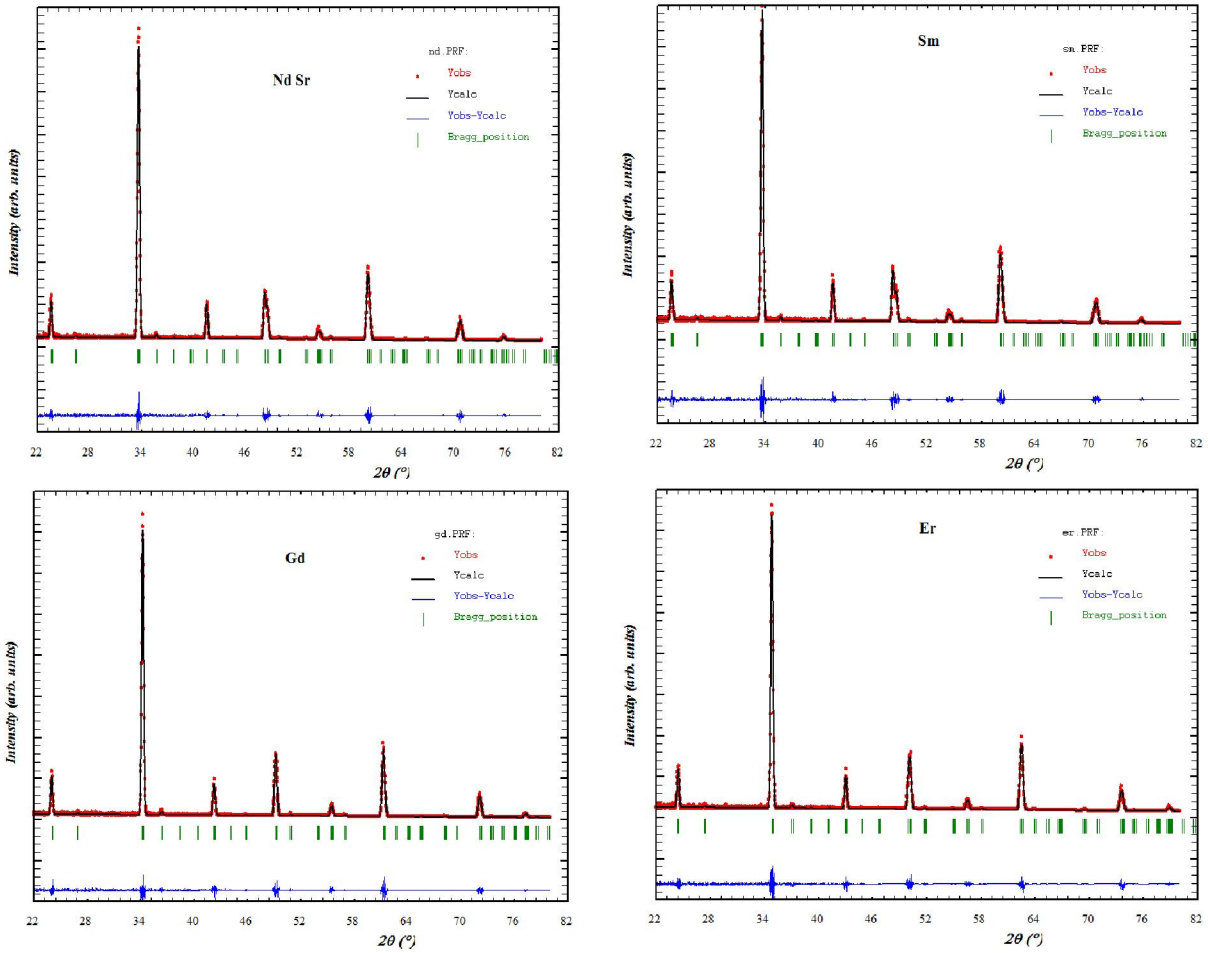

Figure (5). Experimental and refined XRD patterns for $Ln_{0.75}Sr_{0.25}Mn_{0.90}$ $Fe_{0.10}O_3$ where Ln is (Nd^{+3}, Sm^{+3}, Gd^{+3}, or Er^{+3}).

Table (1). Refined structural parameters for the $Ln_{0.75}Sr_{0.25}Mn_{0.90}Fe_{0.10}O_3$ where Ln is (Nd^{+3}, Sm^{+3}, Gd^{+3} and Er^{+3}) i.e. orthorhombic phases. Content: Unit cell dimensions (a, b, c), unit cell volume (V) bond lengths and bond angles for selected bonds, CrySiz D (nm) and ε strain.

Parameters/ samples	Nd	Sm	Gd	Er
ε	0.0496	0.049605	0.04983	0.039915
D	22.33	19.63	15.89	9.63
Lattice Parameters	a=5.3656 b=5.4148 c=7.5917	a=5.3564 b=5.3814 c=7.5792	a=5.3558 b= 5.3654 c=7.5718	a=5.3547 b=5.3458 c=7.5 674
V(Å^3)	220.6	218.5	217.5	216.6
Mn-O	2.15243	2.16243	2.17538	2.18317
Mn-O_2-Mn	170.15587	170.09587	169.75827	169.25175
Tolerance factor	0.9411	0.9336	0.9273	0.9153

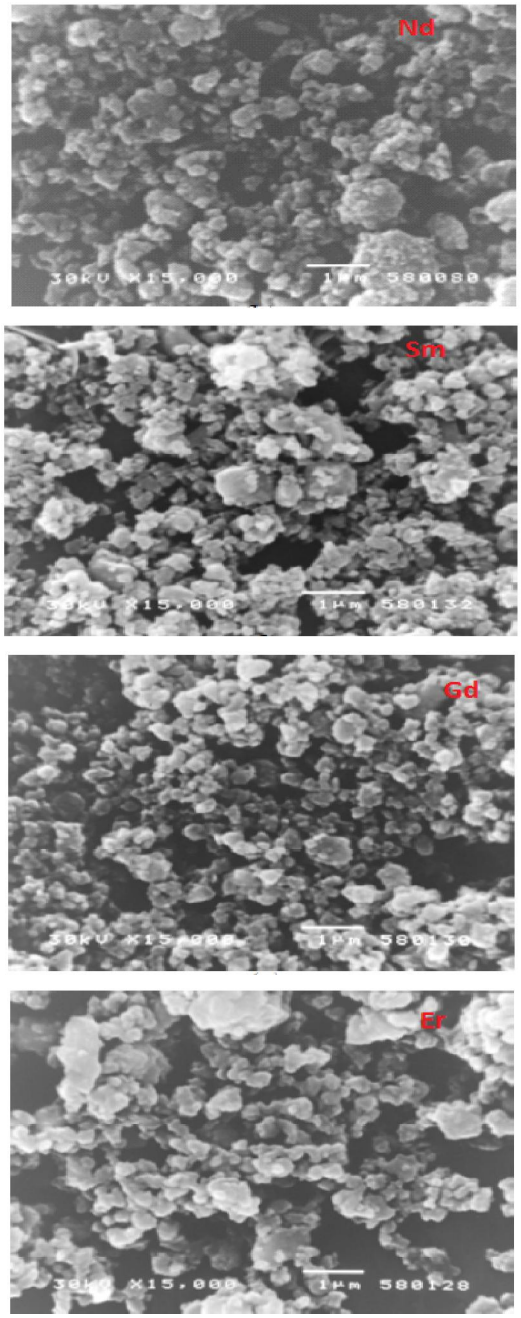

Figure (6). SEM photographs for $Ln_{0.75}Sr_{0.25}Mn_{0.90}Fe_{0.10}O_3$ where Ln is (Nd^{+3}, Sm^{+3}, Gd^{+3} or Er^{+3}).

3.3. BET Specific Surface Area

BET plot for the samples the $Ln_{0.75}Sr_{0.25}Mn_{0.90}Fe_{0.10}O_3$ where Ln is (Nd, Sm, Gd and Er) powders represented in Fig. (7). The calculated surface area for these samples listed in table (2). Fig. (8) shows the evolution in the S_{BET} surface area versus Ln where Ln is (Nd^{+3}, Sm^{+3}, Gd^{+3} or Er^{+3}) of $Ln_{0.75}Sr_{0.25}Mn_{0.90}Fe_{0.10}O_3$. This Figure clearly reveals that sonication produces a remarkable increase in the S_{BET} with Ln where Ln is (Nd^{+3}, Sm^{+3}, Gd^{+3} or Er^{+3}). During the while, the increase of the S_{BET} from (44.94 to 445.4) m2/g. This increase of surface area with Ln can be attributed to the deagglomerate of the particles [14]. This results Compatible with the results of SEM micrographs and Compatible with the results of X-rays diffraction where the particle size decreases with decreasing of the ionic reduce from Nd^{+3} to Er^{+3} of $Ln_{0.75}Sr_{0.25}Mn_{0.90}Fe_{0.10}O_3$ samples where Ln is (Nd^{+3}, Sm^{+3}, Gd^{+3} or Er^{+3}) See Figure (4).

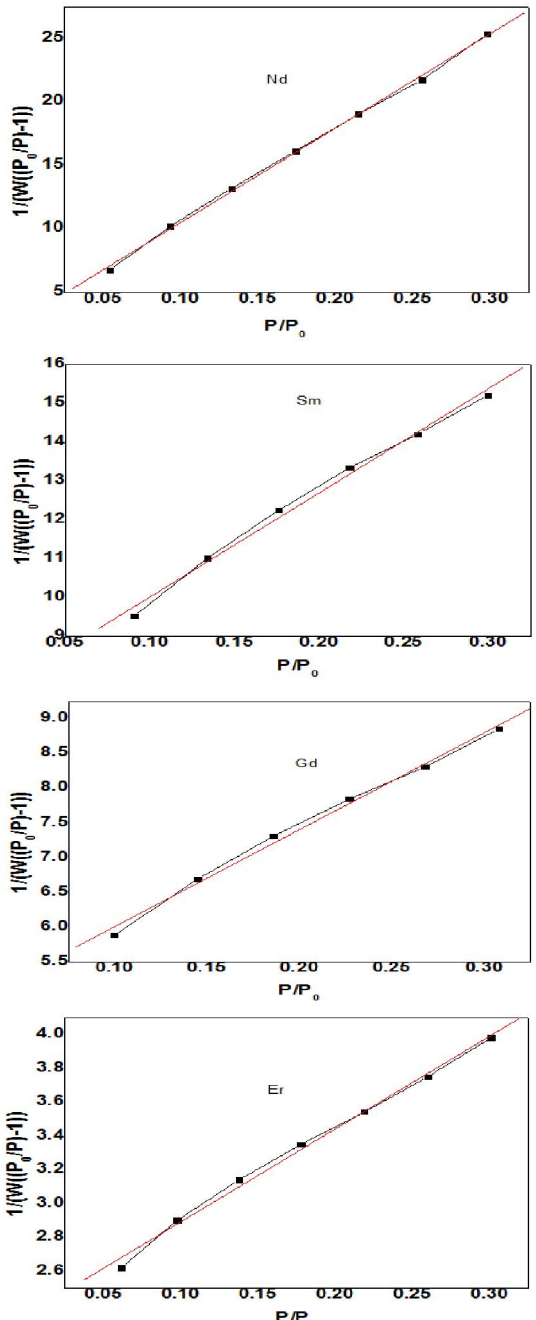

Figure (7) BET plot for $Ln_{0.75}Sr_{0.25}Mn_{0.90}Fe_{0.10}O_3$ samples where Ln is (Nd^{+3}, Sm^{+3}, Gd^{+3} or Er^{+3}).

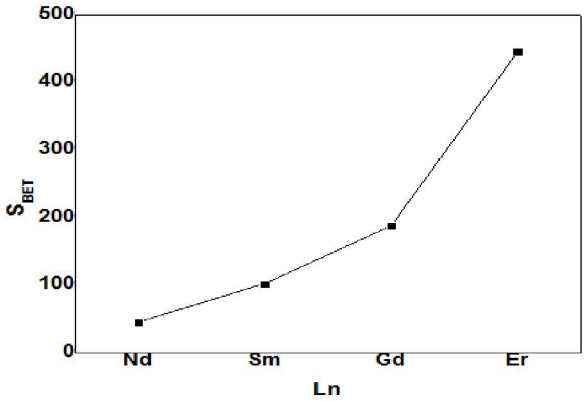

Figure (8). The S_{BET} surface area function in $Ln_{0.75}Sr_{0.25}Mn_{0.90}Fe_{0.10}O_3$ samples where Ln is (Nd^{+3}, Sm^{+3}, Gd^{+3} or Er^{+3}).

Table (2). surface area for $Ln_{0.75}Sr_{0.25}Mn_{0.90}Fe_{0.10}O_3$ samples \ where Ln is (Nd^{+3}, Sm^{+3}, Gd^{+3} or Er^{+3}).

Samples	specific surface area S_{BET} (m2/g)
Nd	44.94
Sm	102
Gd	187.6
Er	445.4

3.4. Magnetic measurements

The hysteresis curves obtained at room temperature with (20k Oe) applied field for a representive sample is shown in Fig. (9). The polycrystalline samples have relatively square hysteresis loops which shows soft ferromagnetic characteristic for all samples. The magnitude of the saturation M_s is increased with substitution of Nd^{+3} by Sm^{3+}, Gd^{3+}, and Er^{+3} in the samples show in Fig. (10). This behavior can be interpreted by decrease in the average radii of A sites and hence to a decrease of the Mn-O-Mn bond angle and a distortion of the MnO_6 octahedrons. This reasons leads to an increase of the double exchange interaction relative to the superexchange interaction and stabilizes the ferromagnetic state. The efficiency of the ferromagnetic double exchange mechanism is tuned by the hopping term of the outer–shell d electrons. Increasing the hybridization between Mn eg and O ^{2}p orbital's favors carrier mobility and hence the double exchange interaction [15]. The obtained magnetic data: coercivity (H_c), permanent (remanence) flux density (Mr) and flux density saturation (M_s) are summarized in the Table (3). From table (3) it can be seen that with substitution of Nd^{+3} by Sm^{3+}, Gd^{3+}, and Er^{+3} in the samples it is found that H_c decreases. This decreases in the coercivity can be attributed to decrease of the grain size where the polycrystalline ferromagnetism, grain boundaries are magnetic domain boundaries. The coercive field decreases with decreasing grain size [16].

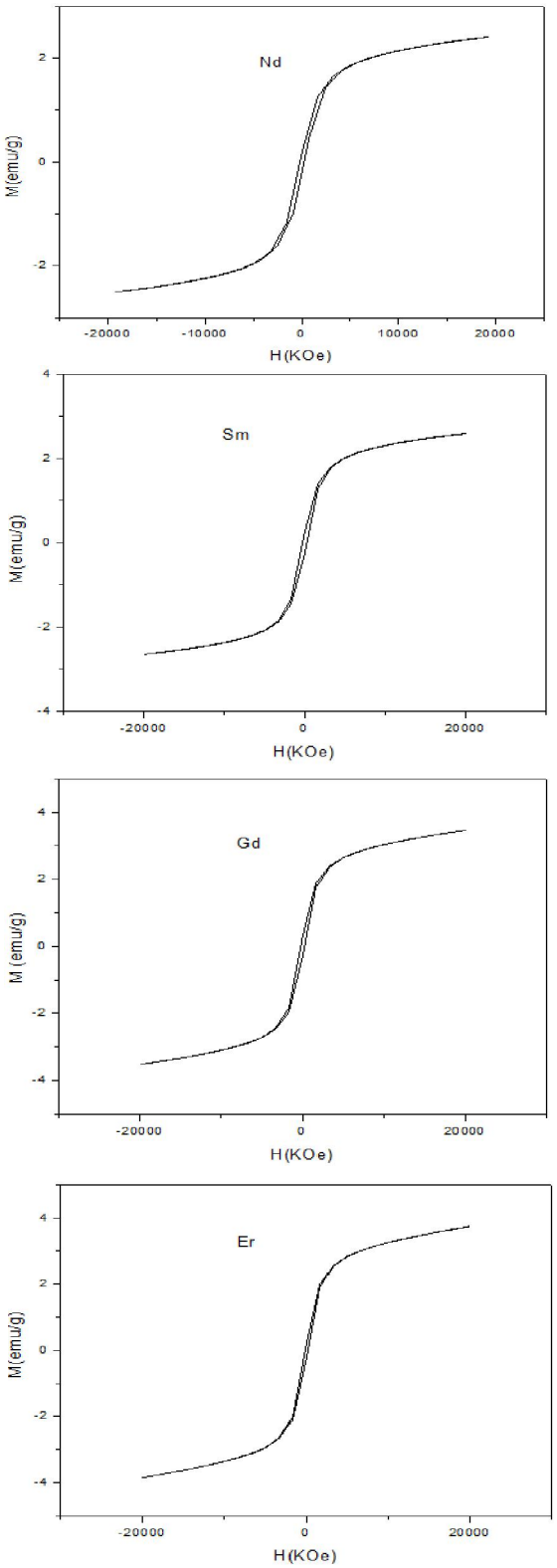

Figure (9). The magnetic hysteresis measurements of $Ln_{0.75}Sr_{0.25}Mn_{0.90}Fe_{0.10}O_3$ samples where Ln is (Nd^{+3}, Sm^{+3}, Gd^{+3}or Er^{+3}) at room temperature with applied field.

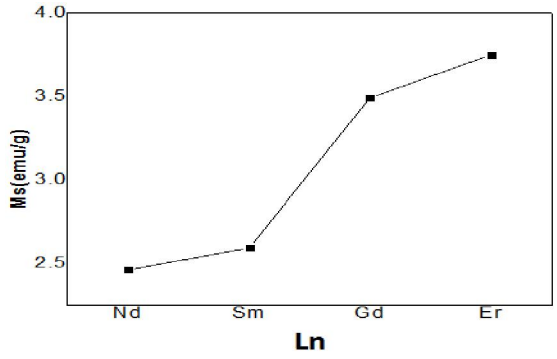

Figure (10). Ms value of $Ln_{0.75}Sr_{0.25}Mn_{0.90}Fe_{0.10}O_3$ samples where Ln is (Nd^{+3}, Sm^{+3}, Gd^{+3} or Er^{+3}).

Table (3). *Ms, Mr* and Hc for the different Ln where Ln is (Nd^{+3}, Sm^{+3}, Gd^{+3} or Er^{+3}).

Ln	Ms (emu/g)	Mr (emu/g)	H (kOe)
Nd	2.4594	0.16809	264
Sm	2.5912	0.20841	228
Gd	3.4899	0.21513	210
Er	3.748	0.2548	159

3.5. Conclusion

The $Ln_{0.75}Sr_{0.25}Mn_{0.90}Fe_{0.10}O_3$ samples with substitution of Nd by similar ionic (Sm, Gd, or Er) content have orthorhombic symmetry (space group pbnm). The Mn-O-Mn bond angle, the particle size and the tolerance factor decreases with substitution of Nd^{+3} by similar ionic (Sm^{+3}, Gd^{+3}, and Er^{+3}). The Mn-O bond distance increase with substitution of Nd^{+3} by similar ionic (Sm^{+3}, Gd^{+3}, or Er^{+3}). This behavior can be interpreted by the decrease in the average radii of A sites. SEM micrographs of powder samples investigation have typical morphology consisting of fine and homogeneous and clearly that with decreasing of the ionic radius from Nd^{+3} to Er^{+3} the particle size decreases. The samples have increased in the specific surface area with decreasing ionic radius from Nd^{+3} to Er^{+3}. These samples have square hysteresis loops which mean that soft ferromagnetic (FM) characteristic. The magnitude of the saturation M_S increased with substitution of Nd^{+3} by similar ionic (Sm^{+3}, Gd^{+3}, and Er^{+3}). This behavior can be interpreted by the decrease in the average radii of A sites.

12/20/2012

Correspondence to:
M. A. Motawea*
Mössbauer Laboratory, Physics Department
Faculty of Science, Al-Azhar University, Nasr City 11884, Cairo, Egypt.
Emails: abdo_metawea@yahoo.com

References

1. E. Dagotto, T. Hotta, A. Moreo, Physics Reports 344 (2001) 1.
2. E.L. Nagaev, Physics Reports 346 (2001) 387
3. J.M.D. Coey, M. Viret, Advances in Physics 48 (1999) 167.
4. A.P. Ramirez, Journal of Physics: Condensed Matter 9 (1997) 8171.
5. J.M. De Teresa, M.R. Ibarra, P.A. Algarabel, C. Ritter, C. Marquina, J. Blasco, J. Garcia, A. de Moral, Z. Arnold, Nature 386 (1997) 256.
6. H. Kawano, R. Kajimoto, H. Yoshizawa, Y. Tomioka, H. Kuwahara, Y. Tokura, Physical Review Letters 78 (1997) 4253
7. C. Suryanarayana, Progress in Materials Science 46 (2001) 1–184.
8. W. Tae Jeong, J. Hyun Joo, K. Sub Lee, Journal of Alloys and Compounds 358 (2003) 294–301.
9. E. Gaffet, F. Bernard, et al., Journal of Materials Chemistry 9 (1999) 305–309.
10. Z. Jin., W. Tang., J. Zhang, Y. Du, Journal of Magnetism and Magnetic Materials 187 (1998) 237.
11. M. Muroi, R. Street, P.G. McCormick, Journal of Applied Physics 87 (2000) 3424.
12. H. Ohbayashi, T. Kudo, and T. Gejo, Jpn. J. Appl. Phys., 13, 1 (1974).
13. B. Hannoyer, G. Marest, J. M. Greneche, Ravi Bathe, S. I. Patil and S. B. Ogale Phys. Rev. B 61, 9613, (2000).
14. D. Dollimore, G.R. Heal, An improved method for the calculation of pore size distribution from adsorption data, J. Appl. Chem. 14 (1964) 109–114.
15. T. Okuda, T. Kimura and Y. Tokura, Phys. Rev. B 60, 3370, (1999).
16. E.artz, Acta Mat. 46, 5611, (1998).